Journal of Biomedical Optics

SPIEDigitalLibrary.org/jbo

Quasi-real-time fluorescence imaging with lifetime dependent contrast

Pei-Chi Jiang
Warren S. Grundfest
Oscar M. Stafsudd

SPIE

Quasi-real-time fluorescence imaging with lifetime dependent contrast

Pei-Chi Jiang,[a] Warren S. Grundfest,[b] and Oscar M. Stafsudd[a]
[a]University of California Los Angeles, Department of Electrical Engineering, Room 18-135 Engineering IV, Los Angeles, California 90095-1594
[b]University of California Los Angeles, Department of Bioengineering, 420 Westwood Plaza, Room 5121 Engineering V, Los Angeles, California 90095-1600

Abstract. Conventional fluorescence lifetime imaging requires complicated algorithms to extract lifetimes of fluorophores and acquisition of multiple data points at progressively longer delay times to characterize tissues. To address diminishing signal-to-noise ratios at these progressively longer time delays, we report a time-resolved fluorescence imaging method, normalized fluorescence yield imaging that does not require the extraction of lifetimes. The concept is to extract the "contrast" instead of the lifetime value of the fluorophores by using simple mathematical algorithms. This process converts differences in decay times directly to different intensities. The technique was verified experimentally using a gated iCCD camera and an ultraviolet light-emitting diode light source. It was shown that this method can distinguish between chemical dyes (Fluorescein and Rhodamine-B) and biomedical samples, such as powders of elastin and collagen. Good contrast was obtained between fluorophores that varied by less than 6% in lifetime. Additionally, it was shown that long gate times up to 16 ns achieve good contrast depending upon the samples to be studied. These results support the feasibility of time-resolved fluorescence imaging without lifetime extraction, which has a potential clinical role in noninvasive real-time imaging. [DOI: 10.1117/1.3609229]

Keywords: time-resolved fluorescence imaging; lifetime extraction; autofluorescence.

Paper 10630R received Nov. 28, 2010; revised manuscript received May 22, 2011; accepted for publication Jun. 6, 2011; published online Aug. 31, 2011.

1 Introduction

Tissue imaging plays a major role in the physician ability to locate tumors and define borders between normal and abnormal tissues. Identification of abnormalities in tissue physiology and composition may allow for improved determination of the location of cancer, identification of failing wounds, and detection of abnormal growth patterns. Development of an accurate rapid method of tissue characterization using optical techniques has the potential to significantly advance patient care.

Studies have shown tissue autofluorescence can provide contrast between different tissue types, such as normal tissues and carcinoma.[1,2] Fluorescence imaging, therefore, is being considered as a method for cancer detection.[3–5] There are two types of fluorescence imaging: steady-state and time-resolved. Steady-state imaging displays, at each pixel of the image, the number of fluorescence photons recorded; time-resolved fluorescence imaging displays, at each pixel, the characteristic decay times of the photons recorded. Steady-state imaging is the most commonly used fluorescence measurement technique due to its simplicity. Time resolved imaging technique requires precisely synchronized measurements on a nanosecond time scale. Steady state fluorescence imaging is limited due to the broad overlapping spectra of many tissue fluorophores. Overlapping spectra limit discrimination between different tissue types. Nonuniform illumination also causes serious problems in intensity detection, particularly for wide-field imaging in medical applications.

Address all correspondence to: Oscar Stafsudd, University of California Los Angeles, Department of Electrical Engineering, Room 18-35 Engineering IV, Los Angeles, California 90095-1594; Tel: 310-825-4360; E-mail: stafsudd@ucla.edu.

Fluorescence lifetime imaging can be obtained using two distinct approaches: in one technique (time-domain), one measures the intensity decay after the sample is exposed to a pulse of light. In a second technique (frequency-domain), the excitation light (continuous wave) is modulated at a frequency f; one measures the phase shift and the demodulation of the fluorescence. The frequency-domain approach can indeed be utilized with pulsed sources as well. In Sec. 2, we will consider mainly the time-domain approach to the determination of fluorescence lifetime imaging (FLIM). FLIM is a common time-resolved fluorescence imaging technique that extracts the fluorescence lifetime from the intensity decays. Lifetimes are extracted from the intensity decay at each pixel, and the image is then generated by assigning an intensity or fast color map to the range of measured lifetime. Since each fluorophore has its unique lifetime, distribution of lifetimes can provide image contrast between different tissues. An advantage of FLIM is that the lifetime measurement is independent of the absolute intensities. This makes the contrast independent of the fluorescence intensity of the emission spectrum, and therefore less sensitive to nonuniform illumination, nonuniform fluorophore concentration, and overlapping emission spectrum.

The fluorescence lifetime is extracted by curve fitting the data of the intensity decay after illumination. For a tissue containing one kind of fluorophore only, the fluorescence decay upon excitation with a narrow pulse of light (ideally a delta-function) can be written as a single-exponential decay:

$$I(t) = A \cdot e^{\frac{-t}{\tau}}, \tag{1}$$

1083-3668/2011/16(8)/086001/9/$25.00 © 2011 SPIE

where A is the amplitude and τ is the lifetime of the decay. Curve fitting can be readily performed in this case. Most biological tissues, however, are composed of more than one fluorophore. This results in a multi-exponential intensity decay, which can be written as follows:

$$I(t) = \sum_n A_n \cdot e^{\frac{-t}{\tau_n}}. \tag{2}$$

Multi-exponential decay has more than one set of amplitudes and lifetimes, which significantly increases the difficulty of the curve-fitting. For example, it has been shown that two exponential decays with different amplitudes and lifetimes cannot be uniquely determined from the data. It has been shown, (Ref. 6)] that two radically different dual exponentials:

$$F(1) = 7500 \cdot e^{\frac{-t}{5.5}} + 2500 \cdot e^{\frac{-t}{8.0}},$$

$$F(2) = 2500 \cdot e^{\frac{-t}{4.5}} + 7500 \cdot e^{\frac{-t}{6.7}},$$

are indistinguishable even in the absence of noise, until the decay curves are three orders of magnitude below their initial levels. This makes it experimentally difficult to uniquely identify the time constants in dual exponentials that are more than 20% different. In addition, it would require signal-to-noise ratios (SNRs) on the order of 10,000 to 1. In addition to fitting complexity, FLIM also suffers from processor intensive technique required for accurate curve fitting. The curve fitting process is required to generate lifetime image and the problem becomes more significant in wide field imaging. This prevents FLIM from being applied to real-time application.

Another problem of FLIM is the consumption of computer time for curve fitting. The curve fitting process has to be done pixel by pixel to generate the lifetime image, and this time-consuming issue becomes even more severe on wide-field imaging. This hinders FLIM from the application of real time and wide-field applications. There are studies that employ algorithms, such as global analysis and stretched exponential fitting, to decrease the processing time.[3,7–9] However, pixel-by-pixel lifetime extraction is still required. The development of a reliable and rapid time-resolved fluorescence imaging method is required to provide real time tissue discrimination and tumor detection.

We present a novel time-resolved fluorescence imaging method which extracts the effect of different lifetimes without the need of curve fitting and lifetime calculations. This method can easily resolve lifetime differences less than 10% and generate effective contrast with modest SNR requirements.

2 Method

2.1 *Theory*

The concept of our method is to map the image with the information of lifetime difference from intensity decays by separating the information from nonideal effects. There are several effects that could interfere with the time-resolved fluorescence experiment, such as: 1. nonuniform illumination, 2. variable fluorescence yield of different tissues, and 3. variable pump absorption by different tissues. The fluorescence decay of a specimen composed of two fluorophores is taken as an example (Fig. 1).

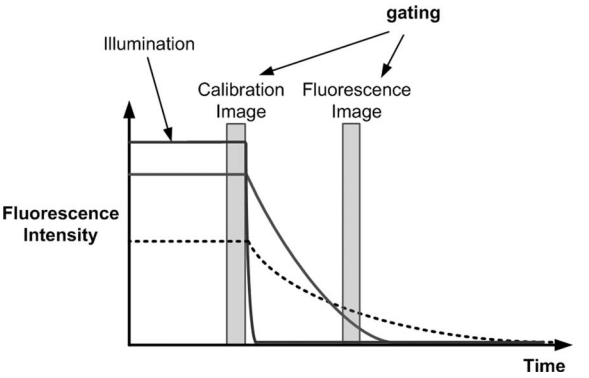

Fig. 1 Fluorescence intensity decays of two fluorophores with different lifetimes (Fluorescence decay of fluorophores with long/short lifetime is demonstrated by gray solid line/ black dot line). The black solid line represents the illumination. Calibration image is recorded during the illumination, while fluorescence image is sampled during the fluorescence decay.

One of the fluorophores has a longer lifetime than that of the other. Unlike conventional FLIM, which records and analyzes the whole intensity decay, only three main images are recorded in our method. The first image is an unexcited dark field, which is used to remove leakage effects, the charge coupled device (CCD) base level, and background illumination via subtraction. The second fluorescence image is taken during excitation, which is referred to as the "calibration image" or "normalization image." The third image is taken during the fluorescence decay. Both the normalization image and the fluorescence decay image have the first "dark field" image subtracted from them. The background corrected fluorescence decay image is divided by the background corrected calibration image. This creates our final image which is therefore normalized for yield point by point.

In principle, normalizing the image taken during decay by the calibration image removes the variation due to nonuniform illumination and/or variation in fluorescent intensity during illumination. The contrast of the image is, therefore, only due to the lifetime differences, or the decay rate. This is a normalized fluorescence yield imaging technique which we call NoFYI.

Figure 2 shows our method, normalized fluorescence yield imaging (NoFYI), graphically. Image 1 is the calibration image and Image 2 is the fluorescence decay image. Both have had the dark image subtracted. The two regions at the left are composed of the shorter-lifetime fluorophore, while those at the right consist of the longer-lifetime fluorophore. If only the intensity values are considered, the specimen seems to have four fluorophores in Image 1 and have two or three fluorophores in Image 2. This is due to the nonuniform illumination and/or variation in fluorescent yield. However, these effects are removed after dividing Image 2 by Image 1, as shown in Image 3. In Image 3, the fluorophores in the specimen can be easily classified. The range of the pixel values can be adjusted by multiplying a constant (Image 4), and the contrast is enhanced by simply adjusting the display range. Because the differences in the decay time have been translated into intensity variation, conventional image processing techniques can be directly applied to these files to enhance the visual appearance of the image.

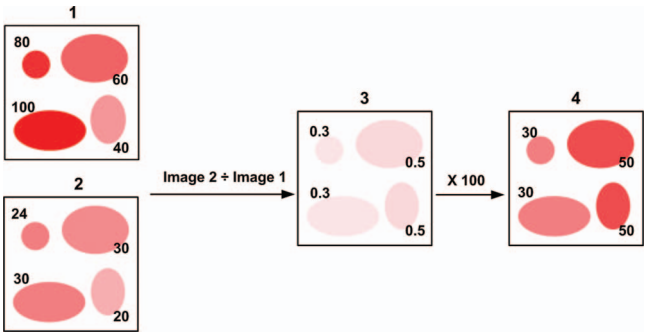

Fig. 2 The procedure of the imaging processing. Image 1 and 2 are the calibration image and fluorescence decay image, respectively. With division of Image 2 by Image 1, classification of the fluorophores can be done (Image 3). Multiplying a constant adjusts the pixel range (Image 4).

Using conventional FLIM techniques, it is necessary to accurately measure the fluorescence decay. This is made difficult by the short decay times encountered in typical tissues. Gate width must be significantly shorter than any time constant to be determined. The short gate times reduce the signal levels and require very expensive gated imagers. NoFYI does not require short gate times although they can be used. Figure 3 demonstrates the fundamental concept.

The signals are proportional to the area under the curves. Clearly, the area difference increases as the gate time increases until τ_{gate} exceeds the longer lifetime. Very long gate time can suffer degradation of the SNR from leakage or background currents. Mathematically, the normalized signals are represented by Eqs. (3) and (4):

$$\text{Signal 1} = \int_{t_1}^{t_2} I_1(t)dt = \int_{t_1}^{t_2} I_0 e^{\frac{-t}{\tau_1}} dt = I_0\tau_1\left(e^{\frac{-t_1}{\tau_1}} - e^{\frac{-t_2}{\tau_1}}\right) \simeq I_0\tau_1 e^{\frac{-t_1}{\tau_1}}, \quad (3)$$

$$\text{Signal 2} = \int_{t_1}^{t_2} I_2(t)dt = \int_{t_1}^{t_2} I_0 e^{\frac{-t}{\tau_2}} dt = I_0\tau_2\left(e^{\frac{-t_1}{\tau_2}} - e^{\frac{-t_2}{\tau_2}}\right) \simeq I_0\tau_2 e^{\frac{-t_1}{\tau_2}}, \quad (4)$$

where I_1 and I_2 are the intensity decays of sample 1 and sample 2, respectively, and τ_1 and τ_2 are the lifetimes. Note that the difference between the two integrations is merely determined by the fluorescence lifetimes, which implies that the contrast of the fluorescence decay image is also due to the lifetimes, even under long gating time. If the gate width exceeds the lifetime and t_1 is short compared to the lifetime, the ratio becomes τ_1/τ_2. If the fluorescence intensity shows a multi-exponential decay, the contrast of the image can also be shown by the difference in the areas under the curves. This proves that NoFYI is robust to gating width, and experimental results demonstrating this are shown in Sec. 2.2.

The main goal of NoFYI is to help increasing the accuracy of target diagnosis and determination. Note that for clinical applications of NoFYI, we usually have the fundamental knowledge of the specimens, and thus measurement of the entire fluorescence decay curves of the samples is not needed. If the information of the specimen is unknown, we only need to measure the decay of a small area or a single point on the specimen to obtain the fundamental nature of the decay, and this data can also be applied to samples of the same kind of tissues in future studies.

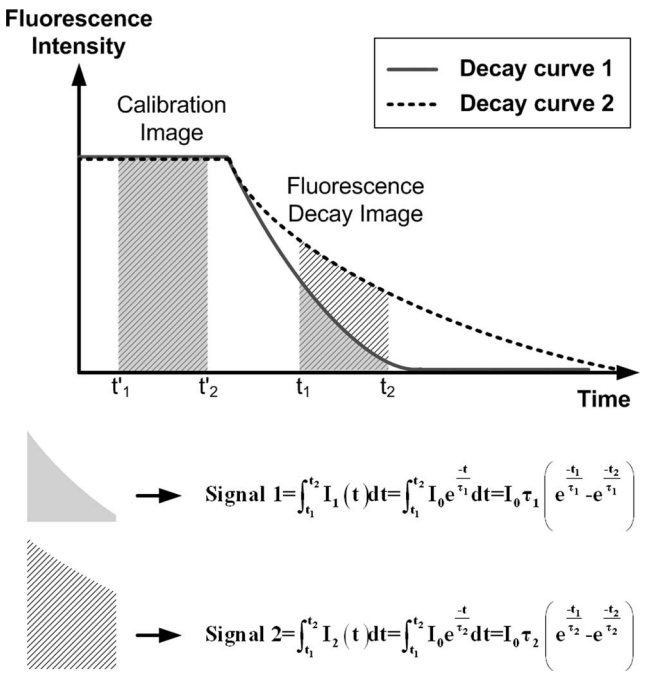

Fig. 3 Time-resolved fluorescence imaging operated under long gate time. Decay curve of fluorophores with long/short gate time is represented by Decay curve 1/2. Slash-line area represent the area under the decay of long gate time, while gray area is that under the decay of short gate time.

2.2 *Experimental Configuration*

Ultraviolet (UV) light-emitting diode (LEDs), instead of lasers, were used for illumination. It has been shown that UV LEDs can be used as the excitation light source for both time-domain and frequency-domain FLIM.[10,11] The light source in our system was composed of two UV LEDs (370 nm, Thorlabs) in series

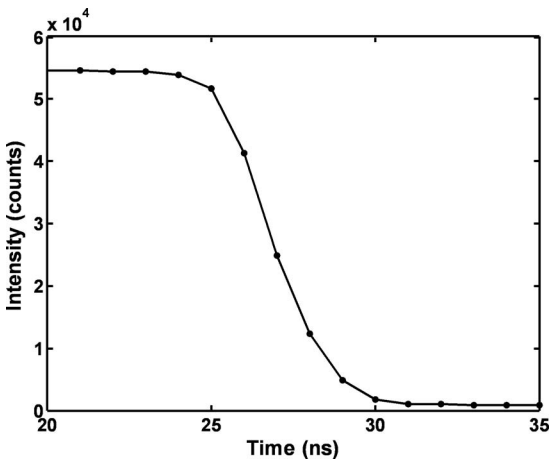

Fig. 4 Intensity curve of the termination of the illumination. Falltime of approximately 6 ns is shown.

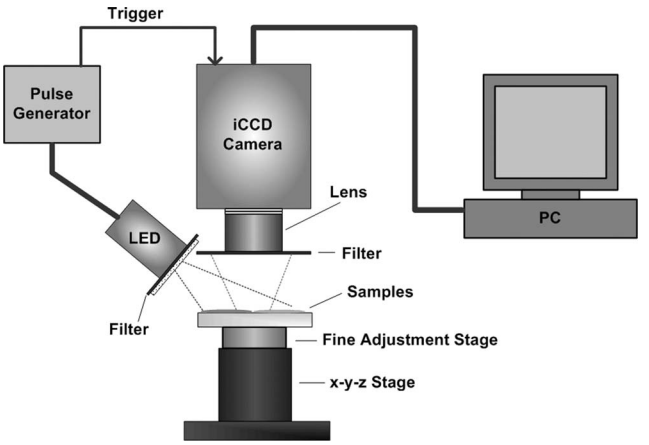

Fig. 5 Schematic diagram of the fluorescence imaging setup.

driven by a pulse generator (HP 8013B). The pulse generator provided 8 V pulses with a 100 ns pulse-width and approximately a 6 ns fall-time (Fig. 4). The repetition rate was set at 20 kHz. The optical peak power is approximately 20 mW and the average power is approximately 40 μW. Employing the UV LEDs simplified the illumination. The small size of LEDs facilitates construction of an array of diodes of different wavelengths, which could be switched on as desired without changing the setup. The pulse width could be controlled and the excitation wavelength can be adjusted by changing to another LED. However, it is possible to get higher excitation power densities with laser illumination compared to the diodes.

Filters were used to separate excitation light and fluorescence signals. The specimens were imaged onto a gated intensified CCD camera which provided a 2 ns gating-width with 1 ns steps between sampling. Note that the 1 ns step width was for the purpose of showing the complete fluorescence decay, and thus around 70 images were acquired for each sample set in this study. In clinical applications, only three images are required to obtain the NoFYI image. The exposure time of the iCCD camera controls the amount of fluorescence being collected, and the gain parameter is in charge of the amplification of the signals. Both parameters were adjusted based on the fluorescence yield of each sample set to obtain the best SNR. The collected fluorescence images were sent to a computer connected to the iCCD camera. The software for image processing was Astroart 4.0.[12] The schematic of the experimental setup is shown in Fig. 5.

The sample was placed on an *x*-*y*-*z* stage for height and direction adjustment. Note the camera can also be directly connected to a typical laboratory microscope by a standard C-mount.

2.3 *Materials*

Chemical dyes and biological powders were used as test samples. The reason for using chemical dyes for the initial test is that dyes provide a known fluorescence lifetime with higher fluorescence intensity. Dyes can also be adjusted in their decay times by the use of different solvents and solvent mixtures and/or concentrations.

Fluorescein and Rhodamin-B (Lambda Physik) dissolved in methanol were chosen as the sample dyes due to their emission fluorescence spectra (in the visible range) and their ease of handling. Because the lifetime of the dye solution changes with concentration, another set of Fluorescein and Rhodamin-B solutions with lower concentrations were used as a comparison. The Fluorescein and Rhodamin-B solutions of higher concentrations (about 1g/L) are labeled FS-H and RB-H, respectively, and the dye solutions of lower concentrations (about 0.5g/L) are labeled FS-L and RB-L.

NoFYI was also tested on biological samples. We tested elastin powders (from bovine neck ligament) and collagen powders (from bovine Achilles tendon), both from the Elastin Products Company.

3 Results

3.1 *Fluorescein and Rhodamin-B*

The time dependent intensity decay of each sample was first recorded by the iCCD camera to obtain the relative decay rate between the samples. The samples were illuminated at 370 nm with a 100 ns-excitation pulse. The iCCD camera sampled the images with a 2 ns gate-width and 1 ns steps between each data point. The starting point of data collection could be controlled so the intensities before and after the illumination could be recorded. The intensity decays of the fluorescence of the dye solutions are shown in Fig. 6.

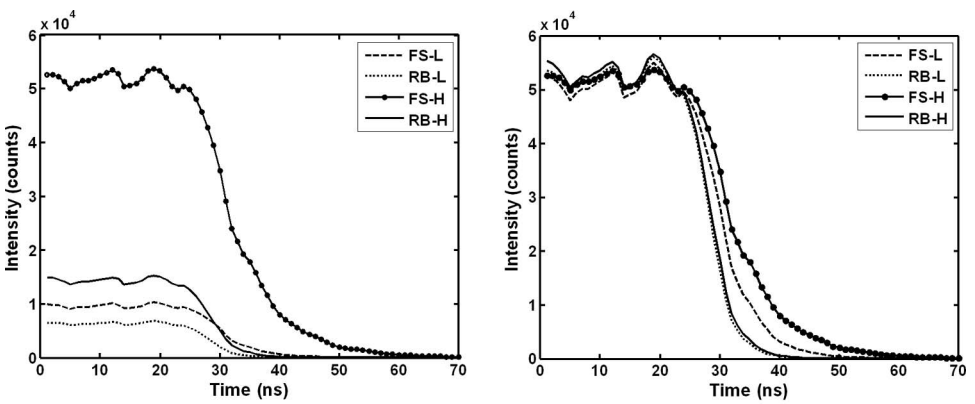

Fig. 6 (a) Fluorescence intensity decays. (b) Normalized intensity decays.

The peak intensities of FS-H and RB-H are higher than those of FS-L and RB-L. Comparing the emittions of Fluorescein and Rhodamin-B, it is apparent that FS-H is more intense than RB-H, and FS-L is more intense than RB-L. Since the pulse generator has an inherent fall-time of approximately 6 ns, the decays appeared to be nonexponential. However, the relative lifetimes between each solution are consistent since fluorescence intensity with longer lifetime decays slower than that with shorter lifetime. In Fig. 6(b), the curves were normalized to match with the initial intensity value of FS-H. It can be seen that Fluorescein obviously has a longer lifetime compared to Rhodamin-B, and solutions with higher concentration have a relatively slower decay rate. Note that the decay rate of RB-H and RB-L are close (2.93 and 2.78 ns, a 5.25% difference).

RB-H and FS-L were chosen as the first sample set. Figure 7(a) shows the unprocessed fluorescence image. RB-H is apparently brighter than FS-L, and the lines shown at the center are the edges of the cuvettes. The division of the fluorescence decay image by the calibration image, shows that the processed image [Fig. 7(b)] successfully discriminates the sample into two clearly determined regions.

The wiremesh plots shown in Figs. 7(c) and 7(d), show not only the large difference in intensity between the two samples after NoFYI processing, but also show the sharpness of the discrimination at the boundary of the two samples. Each pixel on the processed image represents the ratio of emission intensity over calibration intensity. Therefore, fluorophores with longer lifetimes result in higher ratios, which correspond to the brighter pixels; while fluorophores with shorter lifetimes lead to smaller ratio values and thus darker pixels. Since RB-H decays faster than FS-L, the result is consistent with our theory. Note that the darker perimeter in the recorded image is due to nonuniform illumination. These results show NoFYI can easily discriminate between chemical dyes, and is also capable of eliminating the effect of nonuniform illumination.

RB-H and FS-H were chosen as the second sample set. To further assess the impact of nonuniform illumination, we added an optical density (OD 0.2) to block the bottom half of the sample. The intensity distribution, due to partial attenuation, makes the sample looks like a combination of four discrete areas, each composed of different fluorophores, as shown in Fig. 8(a). The result after processing provides a clear discrimination of the two dyes [see Fig. 8(b)].

The entire area of RB-H is much darker than that of FS-H, regardless of the effect of the optical density and the nonuniform illumination at the corner. Figure 8(c) shows the wiremesh plot of the center of the calibration image, which displays the intensity of both RB-H and FS-H with/without attenuation. The successful determination capability of NoFYI can further be emphasized and is demonstrated by the wiremesh plot of the processed image as shown in Fig. 8(d). Despite the nonuniform fluorescence intensity in the calibration image, NoFYI clearly discriminates between the two dyes.

In cases where the lifetimes of the fluorophores are very close in value, an increased contrast can be obtained through spatial averaging. The averaging reduces the effects of noise in the system.

RB-H and RB-L were chosen as the next sample set due to their close lifetimes (2.93 and 2.78 ns). The fluorescence image of this sample set is shown in Fig. 9(a). The NoFYI contrast of

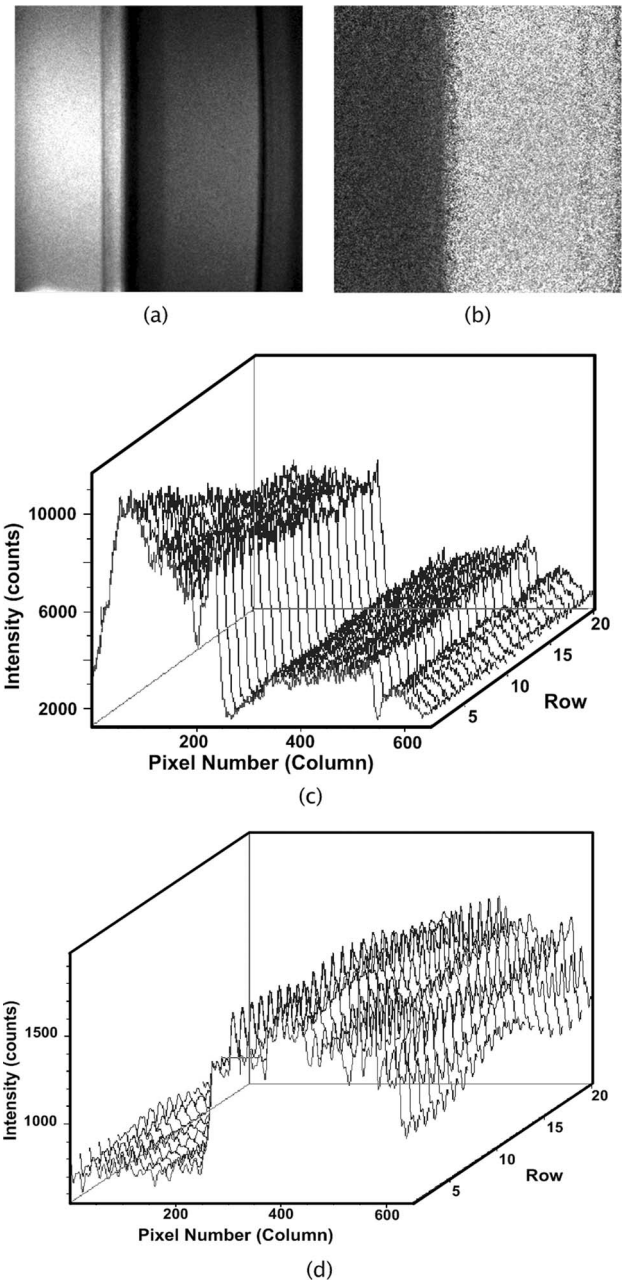

Fig. 7 (a) Unprocessed fluorescence images of RB-H (left) and FS-L (right). (b) Normalized fluorescence image (NoFYI). (c) Wiremesh plot of (a). (Raw fluorescence image). (d) Wiremesh plot of (b). (NoFYI image).

the image is barely visible as seen in Fig. 9(b). Further image processing produces a discernible difference between the two sides of the image despite the close lifetimes.

Since it is already known that RB-L and RB-H are placed at the left and right hand sides respectively, and since both solutions are uniformly distributed on each side, we took the mean of each column by using the "binning" command in Astroart, instead of repeatedly taking the mean of the surrounding eight pixels of each pixel. The NoFYI image was processed by taking the mean of each columns and substituting each pixel by the mean value. In a practical case, repeating spatial averaging is still required to smooth the image and reduce the noise. Figure 9(c) shows

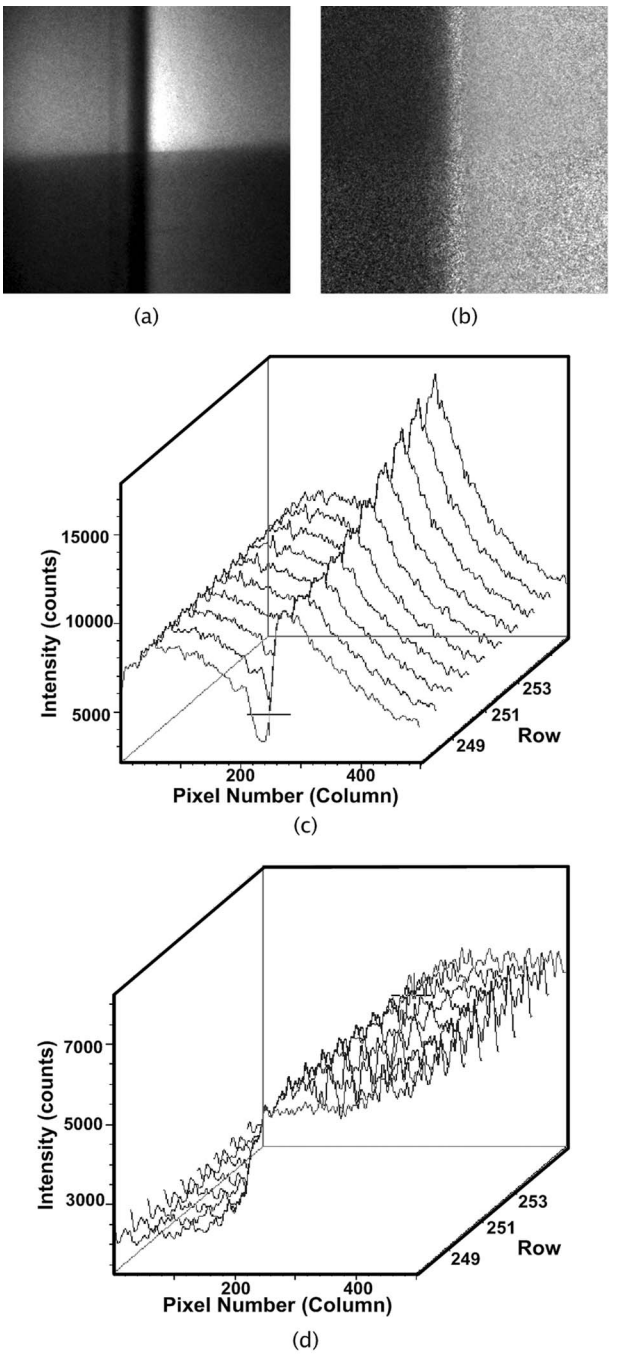

Fig. 8 (a) Unprocessed fluorescence image of RB-H (left) and FS-H (right). (An optical density placed at the bottom for partial attenuation.) (b) NoFYI Processed result of the fluorescence image. (c) Wiremesh plot of part of (a). (Raw fluorescence image) (d) Wiremesh plot of part of (b). (NoFYI image)

the x-profiles of both the calibration image and the processed result. In the x-profile of the processed image [bottom part of Fig. 9(c)], the peak at the center is due to the boundary of the cuvettes, which can be ignored. Comparing the values of the two sides of the peak, a clear intensity difference can be seen. The intensity of RB-L (left) is around 630 counts, while that of RB-H (right) is around 670 counts. The noise variation is lower than 20 counts, which is smaller than the intensity difference between the samples. This shows that NoFYI can produce a measurable

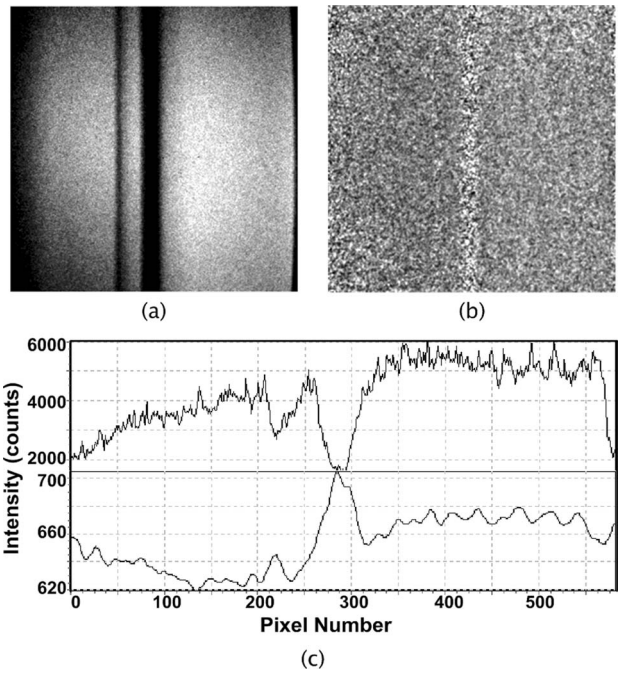

Fig. 9 (a) Unprocessed fluorescence image of RB-L (left) and RB-H (right). (b) Processed NoFYI result. (c) Profiles of (a) (top part) and (b) (bottom part)

contrast image from fluorophores that differ by less than 6% in their lifetimes. Note that the salt and pepper noise appearing in the image mainly results from weak fluorescence signals. This can be improved by increasing the excitation intensity, such as increasing the driving voltage of the LEDs, increasing the number of LEDs, and lengthening the gate times. These images were obtained using modest illumination intensities, i.e. <0.5 mW/cm^2.

3.2 *Long Gate Times*

We also tested NoFYI with different gate times. FS-H and RB-H were chosen as samples. Figure 10(a) shows the fluorescence image of the sample, and the processed images with the gate time of 2, 8, and 16 ns are shown in Figs. 10(b)–10(d). NoFYI clearly determined the two areas using longer gate times. Even if the gate time is longer than the lifetime of the samples, NoFYI continued to provide contrast discrimination between samples. The wiremesh plots of Figs. 10(b)–10(d) are shown in Figs. 10(e)–10(g), respectively. Because long gate times can be successfully used by NoFYI, higher SNRscan be obtained. The feasibility of using long gate times is a feature of time-resolved fluorescence imaging. It lowers the time resolution requirements for the iCCD, and therefore potentially lowers the cost of the setup of the imaging system.

3.3 *Elastin and Collagen*

After showing that NoFYI is able to discriminate chemical dyes without doing lifetime extraction, we investigated the biological powders, elastin, and collagen to observe if NoFYI is capable of discriminating biological samples. Elastin and collagen powders were placed between two sapphire windows and were illuminated by pulse light of 370 nm wavelength with a

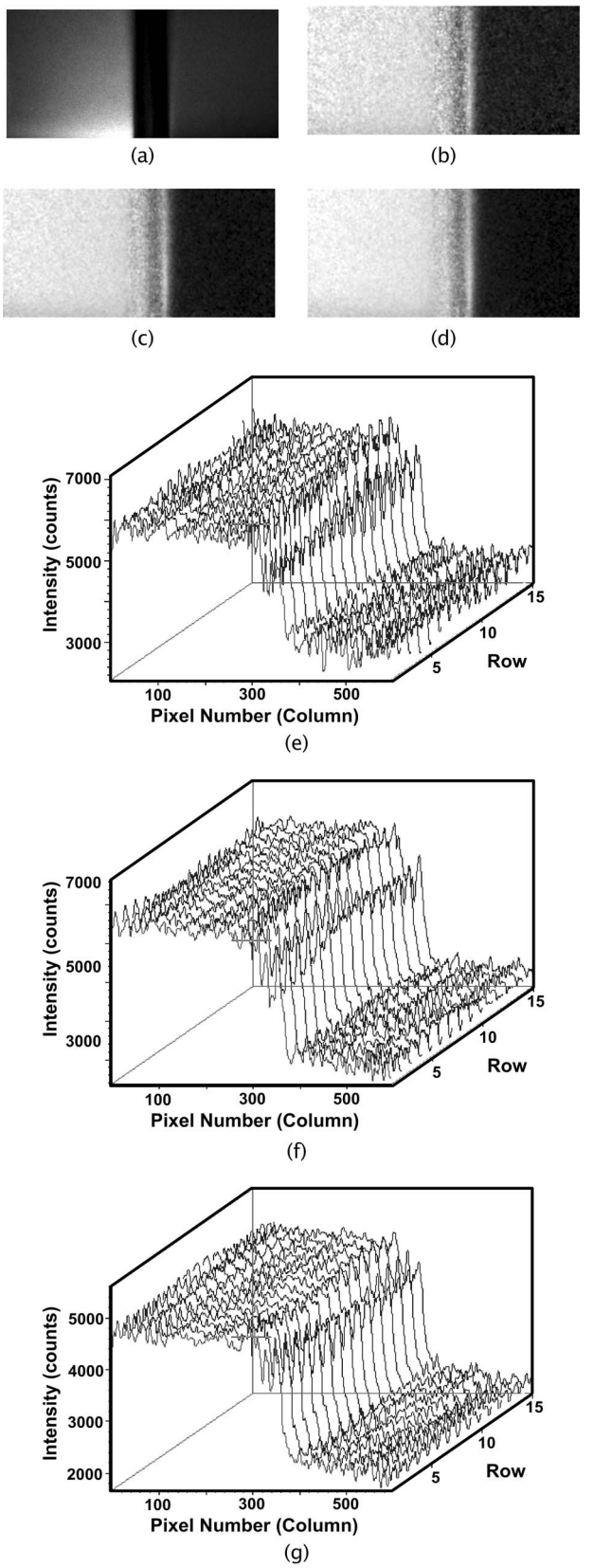

Fig. 10 (a) Fluorescence image of FS-H (left) and RB-H (right) with 2 ns gate time. (b) Processed NoFYI result of (a). (c) Processed NoFYI result with 8 ns gate time. (d) Processed NoFYI result (e) Wiremesh plot of (b). with 16 ns gate time. (f) Wiremesh plot of (c). (g) Wiremesh plot of (d).

100 ns pulse-width. The iCCD camera was operated with 2 and 8 ns gate-widths, and the intensity decays of elastin and collagen powders are shown in Fig. 11. Since the autofluorescence of the sample was weaker than chemical dyes, the exposure time was increased to 5 s to obtain higher contrast. As shown in Fig. 11(a), elastin possessed stronger fluorescence intensity than collagen. The normalized intensity decay [Fig. 11(b)] shows that the intensity of collagen decayed 1 to 2 ns slower than that of elastin.

Figures 12(a) and 12(b) shows the photograph and the fluorescence image of the sample. Most of the areas of elastin powder show similar brightness, while the right hand side of the image is relatively darker, which is the result of nonuniform illumination. The determination of which areas are elastin and collagen cannot therefore be made by observing the contrast in brightness in the original image. However, NoFYI processing of the images (2 ns gate-width) clearly discriminates the two powders as shown in Fig. 12(c).

Elastin has a shorter lifetime which results in relatively darker regions; while the collagen portion of the image became brighter after normalization. Note that NoFYI is also able to preserve the detailed information of the spatial distribution of the samples, even if the fluorescence intensity is much weaker than that of chemical dyes. We also imaged this sample under long gate time condition. Figure 12(d) shows the NoFYI result using 8 ns gate-width, which also successfully discriminates the two powders.

Comparing the two NoFYI images, both images provide clear determination of the two samples, but 8 ns gate-width shows less noise, clearer determination, and higher uniformity. This comparison supports that NoFYI is able to provide clearer determination on bio-samples with long gating time. Note that the noise at the right hand side of the image can be eliminated by adding excitation from the right to achieve uniform illumination.

4 Discussion

In this study, we have demonstrated a novel time-resolved fluorescence imaging method without the need of lifetime extraction. In tissue discrimination, it is the image contrast, instead of the lifetime value, that is the main concern. Therefore, a simple, accurate, and rapid method to extract the contrast is desirable. Employing simple mathematical algorithms such as image subtraction and division, NoFYI has been shown to provide clear sample discrimination and good image quality in wide-field fluorescence imaging without any exponential curve fitting. This eliminates all the undesirable problems resulting from exponential curve fitting, such as arbitrary assumption of single or multiple exponential decay components, time-consuming iterative optimization, and nonunique solutions. Because the NoFYI techniques converts differences in fluorescence decay times to intensity changes, many different commercial image processing programs such as Astroart, Photoshop, etc., can easily be applied to the images.

Lifetimes of the samples were extracted by curve fitting the intensity decays to use as a baseline. The decays of the chemical dyes fit well with a single exponential. Lifetime values range from RB-L (2.78 ns) to RB-H (2.93 ns); FS-L (4.71 ns) to FS-H (7.09 ns). The extracted lifetimes are consistent with the decay rate from the recorded intensity decays as shown in Fig. 6(b).

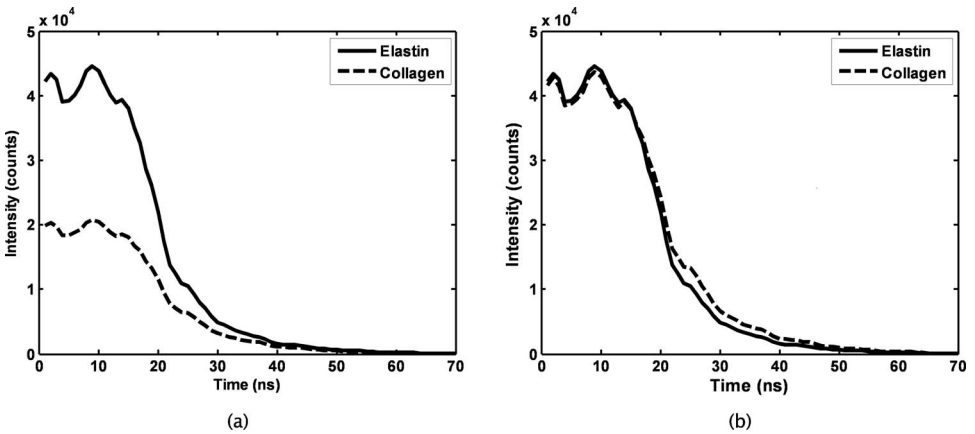

Fig. 11 (a) Fluorescence intensity decays. (b) Normalized intensity decays.

Curve fitting the decays of bio-powders also shows that collagen (3.6 ns) possesses a slightly longer lifetime than elastin (3.0 ns), which matches with the decay curves in Figs. 11(a) and 11(b). Due to the multi-exponential decay of the pump diode output, one obtains a convolution of both the fluorescence sample decay and the diode. While one can extract the actual lifetime of the fluorescence sample, it is relatively difficult. Note that these results not only show that NoFYI is able to discriminate samples with lifetime difference less than 1 ns. Our results demonstrate that the technique works with falltime as long as the lifetime of the fluorescence species. High speed illumination (shorter than 1 ns) is therefore not an requirement of NoFYI for biological imaging. Our experiments show the falltime of the pump need only to be three times the magnitude of the shortest fluorescence lifetime material to be identified. This is an essential advantage since it further lowers the cost of the system and simplifies the operation.

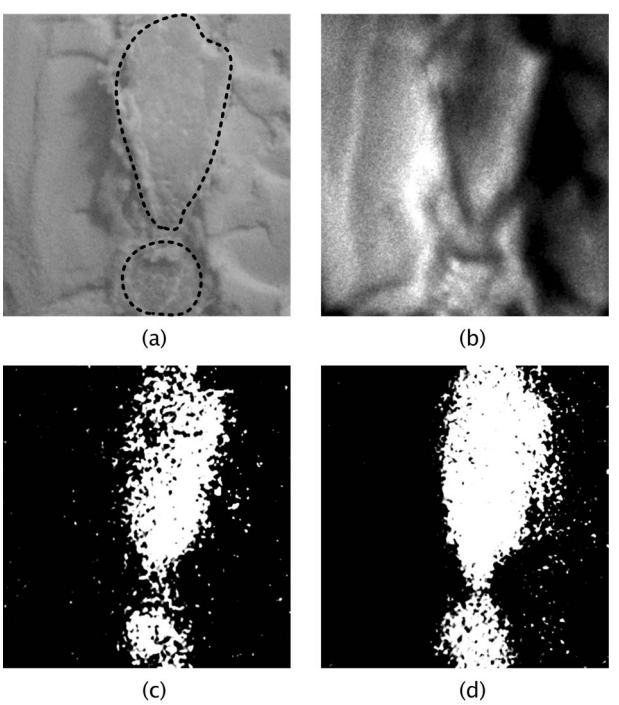

Fig. 12 (a) Photograph of elastin and collagen (dotted circle). (b) Fluorescence image of (a). (c) Processed result (NoFYI image) with 2 ns gate time. (d) Processed result (NoFYI image) with 8 ns gate time.

With respect to the total integration and computational time, NoFYI is more economical than fluorescence lifetime imaging. Due to the simple algorithm, even a wide field image can be processed rapidly. The total integration time of each NoFYI image in this study is around 10 min. Note that this is under the setting of acquiring 70 fluorescence images to show the complete picture of the decay curve. In real uses, we usually have the fundamental knowledge of the specimen so it is not needed to acquire images along the entire decay. Therefore, the total integration time can be reduced to about 1 min since only three images are needed. In cases where the nature of the sample is unknown, we can obtain it by measuring the decays of a small area before applying NoFYI, and this information can also be kept for future studies of the same kind of tissues. The exposure time of the camera is another factor that affects the integration time. For biological samples, since the autofluorescence is weaker than chemical dyes, each fluorescence image requires a longer exposure time than chemical dyes. In the case of elastin and collagen powders, the exposure time was around 5 s to obtain enough fluorescence signals and clear determination of the NoFYI result. However, the acquisition time can be decreased by increasing the gain factor of the camera, while this may also amplify the system noise. An additional solution is to optimize the illumination by increasing the driving voltage of the LEDs and/or increasing the amount of LEDs. Thus, the total integration time can be further shortened to less than 1 min, and quasi-real-time fluorescence imaging can therefore be implemented by using NoFYI.

Besides straight-forward and rapid image processing, another key advantage of NoFYI is the feasibility of long gate times. Using long gate times allows discrimination between the samples with the increase of SNR. Since the feasibility of longer gate time, an iCCD camera with extremely short gate time less than 1 ns is no longer needed, and can be replaced by a lower cost iCCD camera with gating width greater than 2 ns. This feature will reduce the cost of time-resolved fluorescence imaging. So far we have tested longer gating on the sample set such as FS-H/RB-H, FS-L/RB-H, RB-H/RB-L, and elastin and collagen. Among these sample sets, RB-H/RB-L, with a lifetime difference smaller than 1 ns, can still be discriminated success-

fully. In clinical applications, gating time can be designed to serve as a variable of the system during image acquisition for optimization of the image contrast.

With respect to the illumination system, a wide-spectrum tunable-wavelength light source can be constructed by UV LEDs of various emitting wavelengths. Thanks to the development of the semiconductor industry, UV LEDs with emission ranges of 245 to 400 nm are available. Low cost, simple operation, and high power are the benefits of employing UV LEDs in fluorescence imaging. Since the peak absorption wavelength varies with different biological tissues,[11,13] the illumination source should provide for spectral selection.

Previous studies have shown that the combination of temporal and spectral fluorescence information can improve the sensitivity and specificity of fluorescence imaging. It has been demonstrated that time-resolved fluorescence spectroscopy is able to successfully diagnose glioma specimens and characterize different collagen tissues.[4,14] It has also between shown that it enhances the ability of fluorescence measurement on discriminating different grades of atherosclerotic lesions.[15,16] Future work will optimize NoFYI imaging through the use of multiple wavelength LED illumination and bandpass filters to discriminate the fluorescence wavelengths.

It should be noted that an alternative technique, frequency-domain FLIM, has been developed using a sinusoidal modulated pump source and a similarly modulated image intensifier. This technique can be used to recover images in such a way to identify areas with different lifetimes.[17–19] Gioux et al. have shown that lifetime varying from 0.5 to 1.5 ns can be resolved spatially by this technique.

5 Conclusion

In this study, we show a time-resolved fluorescence imaging method (NoFYI) without the need of lifetime extraction. It is capable of discriminating between various chemical dyes (Fluorescein and Rhodamin-B), elastin, and collagen powders. NoFYI is a wide-field imaging technique which extracts lifetime information in the form of intensity differences or contrast, and therefore does not require separate time intensive calculations for each image pixel, nor the measurement of many images with discrete time delays. The ability of NoFYI to operate with light source falltime as long as around three times the shortest fluorophore lifetime and with gate times as much as five times the shortest lifetime reduces the system requirements drastically with respect to device performance. Therefore, NoFYI not only reduces drastically the computer time, but also eases the requirement of pumping light generation and gated imager performance. This makes it possible to have a quasi-real time cost effective lifetime discriminating fluorescence imaging system.

References

1. I. Bliznakova, E. Borisova, and L. Avramov, "Laser and light-induced autofluorescence spectroscopy of human skin in dependence on excitation wavelengths," *Acta. Physica. Polonica A* **112**(5), 1131–1136 (2007).
2. Z. W. Huang, W. Zheng, S. S. Xie, R. Chen, H. Zeng, D. I. McLean, and H. Liu, "Laser-induced autofluorescence microscopy of normal and tumor human colonic tissue," *Int. J. Oncol.* **24**(1), 59–63 (2004).
3. N. P. Galletly, J. McGinty, C. Dunsby, F. Teixieira, J. Requejo-Isidro, I. Munro, D. S. Elson, M. A. A. Neil, A. C. Chu, P. M. W. French, and G. W. Stamp, "Fluorescence lifetime imaging distinguishes basal cell carcinoma from surrounding uninvolved skin," *Br. J. Dermatol.* **159**(1), 152–161 (2008).
4. W. H. Yong, P. V. Butte, B. K. Pikul, J. A. Jo, Q. Fang, T. Papaioannou, K. L. Black, and L. Marcu, "Distinction of brain tissue, low grade and high grade glioma with time-resolved fluorescence spectroscopy," *Front, Biosci.* **11**, 1255–1263 (2006).
5. R. Cubeddu, A. Pifferi, P. Taroni, G. Valentini, F. Rinaldi, and E. Sorbellini, et al., "Fluorescence lifetime imaging: an application to the detection of skin tumors," *IEEE J. Sel. Top. Quantum Electron.*, **5**(4), 923–929 (1999).
6. J. Lakowicz, "Time-domain lifetime measurements," Chapter 4 in *Principles of Fluorescence Spectroscopy*, pp. 98–154, 3 ed., Springer, New York (2006).
7. P. R. Barber, S. M. Ameer-Beg, J. Gilbey, R. J. Edens, I. Ezike, and B. Vojnovic, "Global and pixel kinetic data analysis for FRET detection by multi-photon time-domain FLIM," *Proc. SPIE* **5700**, 171–181 (2005).
8. T. Eruv, M. Ben-David, and I. Gannot, "An alternative approach to analyze fluorescence lifetime images as a base for a tumor early diagnosis system," *IEEE J. Sel. Top. Quantum Electron.* **14**(1), 98–104 (2008).
9. K. C. B. Lee, J. Siegel, S. E. D. Webb, S. Leveque-Fort, M. J. Cole, R. Jones, K. Dowling, M. J. Lever, and P. M. W. French, "Application of the stretched exponential function to fluorescence lifetime imaging," *Biophys. J.* **81**(3), 1265–1274 (2001).
10. G. T. Kennedy, D. S. Elson, J. D. Hares, I. Munro, V. Poher, P. M. W. French, and M. A. A. Neil, "Fluorescence lifetime imaging using light emitting diodes," *J. Phys, D.* **41**(9), 094012 (2008).
11. P. Herman, B. P. Maliwal, H. J. Lin, and J. R. Lakowicz, "Frequency-domain fluorescence microscopy with the LED as a light source," *J. Microsc.* **203**, 176–181 (2001).
12. G. Parker, "Computational considerations – data acquisition and image processing," Chapter 4 in *Making Beautiful Deep-Sky Images: Astrophotography With Affordable Equipment and Software*, pp. 39–43, Springer, New York (2007).
13. L. Bachmann, D. M. Zezell, A. D. Ribeiro, L. Gomes, and A. S. Ito, "Fluorescence spectroscopy of biological tissues - A review," *Appl. Spectrosc. Rev.* **41**(6), 575–590 (2006).
14. J. M. I. Maarek, L. Marcu, W. J. Snyder, and W. S. Grundfest, "Time-resolved fluorescence spectra of arterial fluorescent compounds: reconstruction with the laguerre expansion technique," *Photochem. Photobiol.* **71**(2), 178–187 (2000).
15. L. Marcu, M. C. Fishbein, J. M. I. Maarek, and W. S. Grundfest, "Discrimination of human coronary artery atherosclerotic lipid-rich lesions by time-resolved laser-induced fluorescence spectroscopy," *Arterioscler. Thromb. Vasc. Biol.* **21**(7), 1244–1250 (2001).
16. L. Marcu, Q. Y. Fang, J. A. Jo, T. Papaioannou, A. Dorafshar, T. Reil, J. H. Qiao, J. D. Baker, J. A. Freischlag, and M. C. Fishbein, "*In vivo* detection of macrophages in a rabbit atherosclerotic model by time-resolved laser-induced fluorescence spectroscopy," *Atherosclerosis* **181**(2), 295–303 (2005).
17. S. Gioux, S. J. Lomnes, H. S. Choi, and J. V. Frangioni, "Low-frequency wide-field fluorescence lifetime imaging using a high-power near-infrared light-emitting diode light source," *J. Biomed. Opt.* **15**(2), 026005 (2010).
18. E. B. van Munster, J. Goedhart, G. J. Kremers, E. M. Menders, and T. W. J. Gadella, "Combination of a spinning disc confocal unit with frequency-domain fluorescence lifetime imaging microscopy," *Cytometry, Part A*, **71A**(4), 207–214 (2007).
19. E. B. van Munster and T. W. J. Gadella, "Fluorescence lifetime imaging microscopy (FLIM)," *Microscopy Techniques* **95**, 143–175 (2005).